Biochemical and Biophysical Research Communications 446 (2014) 352–357

Contents lists available at ScienceDirect

Biochemical and Biophysical Research Communications

journal homepage: www.elsevier.com/locate/ybbrc

Molecular determinants of the interaction between Doa1 and Hse1 involved in endosomal sorting

Seungsu Han, Donghyuk Shin, Hoon Choi, Sangho Lee *

Department of Biological Sciences, Sungkyunkwan University, Suwon 440-746, South Korea

ARTICLE INFO

Article history:
Received 22 February 2014
Available online 4 March 2014

Keywords:
Doa1
Hse1
PFU
SH3
Interaction
Endosomal sorting

ABSTRACT

Yeast Doa1/Ufd3 is an adaptor protein for Cdc48 (p97 in mammal), an AAA type ATPase associated with endoplasmic reticulum-associated protein degradation pathway and endosomal sorting into multivesicular bodies. Doa1 functions in the endosomal sorting by its association with Hse1, a component of endosomal sorting complex required for transport (ESCRT) system. The association of Doa1 with Hse1 was previously reported to be mediated between PFU domain of Doa1 and SH3 of Hse1. However, it remains unclear which residues are specifically involved in the interaction. Here we report that Doa1/PFU interacts with Hse1/SH3 with a moderate affinity of 5 μM. Asn-438 of Doa1/PFU and Trp-254 of Hse1/SH3 are found to be critical in the interaction while Phe-434, implicated in ubiquitin binding via a hydrophobic interaction, is not. Small-angle X-ray scattering measurements combined with molecular docking and biochemical analysis yield the solution structure of the Doa1/PFU:Hse1/SH3 complex. Taken together, our results suggest that hydrogen bonding is a major determinant in the interaction of Doa1/PFU with Hse1/SH3.

1. Introduction

Doa1 (degradation of α2 1)/Ufd3 (ubiquitin fusion degradation 3) was first found in genetic screening in *Saccharomyces cerevisiae* for defects in proteasomal degradation of MATα2 transcription repressor [1]. Major functions of Doa1 and its mammalian ortholog phosphoslipase A2-associating protein (PLAA) are believed to play a role in ubiquitin-dependent proteasomal degradation and to maintain ubiquitin homeostasis in cell. Other functions of Doa1 include involvement in DNA damage response in yeast [2], growth temperature and morphology in fungus *Candida albicans* [3], and cell cycle progression [4]. Doa1 consists of three domains: WD40 domain at the N-terminus, PLAA family ubiquitin-binding (PFU) domain in the middle and PLAA, Ufd3 and Lub1 (PUL) domain at the C-terminus.

The cellular functions of Doa1 are mainly mediated by interactions of the domains in Doa1 with other proteins. Doa1 interacts with cell division cycle protein 48 (Cdc48; p97/VCP in mammals) [1]. By interaction with Cdc48, Doa1 serves as an adapter for Cdc48 which in turn functions in endoplasmic reticulum-associated degradation. Structural and biochemical studies revealed that Doa1 and PLAA interact with ubiquitin via its WD40 and PFU domains [5–7]. The PFU domain of yeast Doa1 binds both monoubiquitin and K29-linked polyubiquitin [5,8]. Binding of the PFU domain of human PLAA to monoubiquitin is very weak with K_d being about 1 mM, which is detectable by a very sensitive biophysical technique such as nuclear magnetic resonance (NMR) [6]. The WD40 domain of yeast Doa1 binds monoubiquitin with a higher affinity ($K_d \sim 200$ μM) determined by NMR [7].

A recent study unveiled a new functional role of Doa1 in endosomal sorting by association with Hse1, a component of endosomal sorting complex required for transport (ESCRT) system [9]. The ESCRT system is involved in biogenesis of multivesicular bodies (MVBs) on endosomal membrane, which finally sort the ubiquitinated membrane protein to vacuole/lysosome for degradation [10]. The association between Doa1 and Hse1 is reported to be achieved by the PFU domain of Doa1 and SH3 domain of Hse1. Loss of Doa1 impairs sorting ubiquitinated membrane proteins to yeast vacuoles, establishing the functional link between Doa1 and MVB pathway [9]. Despite the biological significance of the interaction between Doa1 and Hse through PFU and SH3 domains, limited information is available about the biochemical and molecular basis for such an interaction. For instance, two Trp residues ($W^{254}W^{255}$) of Hse1–SH3 domain are known to be critical in the interaction with Doa1/PFU [9]. Residues 433–445 of Doa1 are involved in the interaction with Hse1/SH3 domain [9,11]. Crystallographic analysis revealed that residues 434–441 form a conserved hydrophobic

* Corresponding author. Fax: +82 502 302 0772.
E-mail address: sangholee@skku.edu (S. Lee).

http://dx.doi.org/10.1016/j.bbrc.2014.02.118
0006-291X/

pocket [12], suggesting that the interaction between Doa1/PFU and Hse1/SH3 may be mediated by hydrophobic interactions. However, it is unclear which specific residues are involved in the interaction between Doa1/PFU and Hse1/SH3. To elucidate the nature of the association between Doa1 and Hse1, we investigated the interaction between the PFU domain of Doa1 and SH3 domain of Hse1 *in vitro* using a combination of biochemical and biophysical techniques. Surprisingly, we found that two residues, N438 of Doa1 and W254 of Hse1, are critical for the interaction by hydrogen bonding, not a hydrophobic interaction. Furthermore, we derived the solution structural model of Doa1 and Hse1 complex.

2. Materials and methods

2.1. Cloning and mutagenesis

Genes encoding yeast Doa1$_{296–450,\ 331–450}$ (PFU domain) and Hse1$_{200–300,\ 217–276}$ (SH3 domain) were amplified using Pfu polymerase (SolGent). Primers for amplification of Doa1 gene were designed to add the HA tag (YPYDVPDYA) at the C-terminus of Doa1. The PCR products were cloned into parallel GST vector and His vector [13]. Primers for site-directed mutagenesis of Doa1$_{296–450}$ mutants (F434A, F434D, N438A, and N440A) and Hse1$_{200–300}$ mutant (W254A) were designed by QuikChange II primer design program on Agilent Technologies website (http://www.genomics.agilent.com). *Dpn*I (New England Biolabs) was used to remove the template DNA vector. Identities of all constructs and mutants were confirmed by DNA sequencing.

2.2. Protein expression and purification

All proteins used for this study were overexpressed in *Escherichia coli* BL21(DE3) strain. Cells were grown at 37 °C until OD_{600} reached 0.6 at which gene expression was induced with 0.1 mM IPTG. The induced cells were further incubated for 20 h at 16 °C with gentle agitation. The cells were harvested by centrifugation, resuspended in 40 ml buffer A (50 mM Tris–HCl pH 7.5 and 150 mM NaCl) and lysed by unltrasonication. The lysate including His-Doa1$_{296–450}$-HA was centrifuged and the supernatant was loaded to Ni-NTA agarose resin (Qiagen). The resin was washed with buffer B (50 mM Tris–HCl pH 7.5, 500 mM NaCl, and 20 mM imidazole) and the bound protein was eluted in buffer C (50 mM Tris–HCl pH 7.5, 500 mM NaCl, and 300 mM imidazole). The cell lysates including GST-Hse1$_{200–300}$ and GST as a control were also centrifuged and each supernatant was loaded to glutathione-Sepharose resin (GE Healthcare). The resin was washed with the buffer A and each bound protein was eluted in buffer D (10 mM Tris–Cl pH 8.0 and 10 mM reduced glutathione). The eluted proteins were further purified by size exclusion chromatography on a HiLoad 16/60 Superdex 200 prep grade (GE Healthcare) column pre-equilibrated with the buffer A. Purity of purified proteins was analyzed by SDS–PAGE.

2.3. Pulldown

Purified 100 pmol of GST or GST-Hse1$_{200–300}$ was loaded to 30 μl of 50% slurry of glutathione-Sepharose beads (GE Healthcare) pre-equilibrated with the buffer A. After incubation for 30 min at room temperature with gently mixing, the beads were washed out with 500 μl of the buffer A to remove unbound proteins. 500 pmol of His-Doa1$_{296–450}$-HA was then applied to the beads and incubated at 4 °C for 2 h. The beads were washed with buffer E (50 mM Tris–HCl pH 7.5, 300 mM NaCl, and 1% (v/v) NP-40). Samples were analyzed by SDS–PAGE and immunoblotting.

2.4. Biolayer interferometry (BLI)

BLI measurements were performed on a BLItz system (ForteBio). Ni-NTA biosensors (ForteBio) were used to immobilize His-Doa1$_{296–450}$-HA proteins. Sensors were pre-wetted in the buffer A for 10 min prior to protein immobilization. His-Doa1$_{296–450}$-HA at 10 μM was immobilized to the sensors through Ni-6xHis interaction. Then, the sensors were washed with the buffer A and reacted with various concentrations (from 2 to 32 μM) of GST-Hse1$_{200–300}$ for association steps. After association reached to equilibrium, the sensor was moved to the buffer A for dissociation steps. GST protein was used as the reference in the association step. Steady state analysis was performed using *Prism* (GraphPad Software Inc.) to calculate the K_d values. R^2, a quantitative indication of goodness of curve fitting, was calculated by the equation $R^2 = 1.0 - (wSS_{model}/wSS_{horizontal})$, where wSS_{model} is the weighted sum-of-squares of the residuals from the model and $wSS_{horizontal}$ is the weighted sum-of-squares of the residuals from the null hypothesis model. The R^2 for analysis was above 0.97. All measurements using mutants of Doa1 and Hse1 were performed in the same way.

2.5. Protein structure modeling

Structural models for Doa1$_{331–450}$ and Hse1$_{217–276}$ were generated by a hybrid approach. For Doa1, residues 376–439 were imported from the crystal structure of PFU domain (PDB ID: 3L3F) with other regions modelled by *ab initio* modeling using *Rosetta* [14]. Hse1$_{217–276}$, corresponding to SH3 domain defined by UniProt [15], was modelled by *GalaxyTBM* [16]. We used the best structure model which was selected automatically by the *GalaxyTBM* out of 5 model candidates. A model for the Doa1/PFU:Hse1/SH3 complex was derived by *HADDOCK* webserver [17] with the following key residues identified by BLI analysis as restraints: N438 of Doa1 and W254 of Hse1.

2.6. Small-angle X-ray scattering (SAXS) data collection and analysis

Truncated constructs, His-Doa1$_{331–450}$-HA and GST-Hse1$_{217–276}$, were used to obtain a stable and well-behaving complex suitable for SAXS measurements. Flexible loop regions for truncation in Doa1/PFU and Hse1/SH3, residues 296–330 and 200–216, respectively, were predicted by *Phyre2* fold recognition server [18]. His-tag and GST were removed after affinity chromatography by TEV (tobacco etch virus) protease and mixed to form a complex. The resulting complex was further purified by size exclusion chromatography. The purified protein complex was then concentrated up to 3.6 mg/ml in the buffer A supplemented with 1 mM DTT. SAXS data collection was performed at the 4C beamline of the Pohang Accelerator Laboratory in Korea. Data collection and processing statistics are listed in Table 2. The buffer A supplemented with 1 mM DTT was used as the reference. SAXS patterns were collected 5 times and monitored whether protein sample had radiation damage. The radii of gyration (R_g) were calculated from the Guinier plot: $I(s) \cong I(0)\exp\left(-\frac{1}{3}R_g^2q^2\right)$. Scattering profiles ($I(q)$) were converted to distance distribution function ($P(r)$) though indirect Fourier transform using *GNOM* [19].

2.7. Derivation of solution structure of Doa1:Hse1 complex

Ten *ab initio* low-resolution envelope shapes for the Doa1$_{331–450}$-HA and Hse1$_{217–276}$ complex were generated by *DAMMIF* [20]. Rigid body modeling of the *HADDOCK*-derived complex model of Doa1$_{331–450}$ and Hse1$_{217–276}$ into the SAXS-derived envelopes was performed by *BUNCH* [21]. The *HADDOCK*-derived complex model was compared to each *ab initio* envelope to choose the

best-fit envelope model. The *Phyre2*-predicted flexible loops and HA-tag in Doa1$_{331–450}$-HA were also considered as loops and *BUNCH* determined their positions. The resulting rigid body model was validated using *FoXS* webserver [22] that fitted model-based calculated scattering profile to experimental one. Conformational dynamics was modeled by *EOM* [23,24], which suggested 5 candidate conformers. The *FoXS* webserver determined the best two models from the candidates using a minimal ensemble search (*MES*) algorithm [25] and validated whether this ensemble fits to experimental scattering patterns.

3. Results

Doa1 reportedly binds to Hse1 via the interaction between PFU domain of Doa1 and SH3 domain of Hse1 [9]. To characterize the interaction between PFU and SH3 domains biochemically, we prepared constructs covering Doa1/PFU and Hse1/SH3, respectively (Fig. 1A). Doa1 construct encompasses residues 296–450 that cover the previously defined minimal SH3-binding region (residues 426–445) [9]. Hse1 construct (residues 200–300) contains SH3 domain (residues 217–276). For ease of purification and differential detection, we added a hexa-histidine tag at the N-terminus and HA-tag at the C-terminus of Doa1$_{296–450}$ (termed His-Doa1$_{296–450}$-HA) and a glutathione *S*-transferase (GST) at the N-terminus of Hse1$_{200–300}$ (termed GST-Hse1$_{200–300}$). We confirmed the reported direct interaction between Doa1/PFU and Hse1/SH3 by GST pulldown assay using purified GST-Hse1$_{200–300}$ and His-Doa1$_{296–450}$-HA (Fig. 1B). As expected, GST-Hse1$_{200–300}$ binds to His-Doa1$_{296–450}$-HA specifically. Such a result implicates that Hse1$_{200–300}$ and Doa1$_{296–450}$ may be able to form a stable complex *in vitro*.

To study whether His-Doa1$_{296–450}$-HA forms a stable complex with GST-Hse1$_{200–300}$ in solution, we employed size exclusion chromatography (Fig. 2). Doa1$_{296–450}$-HA was eluted at a calculated molecular weight of 23 kDa and Hse1$_{200–300}$ at 14 kDa. By contrast, Doa1$_{296–450}$-HA:Hse1$_{200–300}$ complex was eluted at a shifted volume corresponding to a calculated molecular weight of 32 kDa. This indicates that Doa1$_{296–450}$-HA:Hse1$_{200–300}$ complex is stable in solution and the binding stoichiometry is 1:1. Considering that only Doa1 contains a small, 9-residue-long HA tag, we conclude

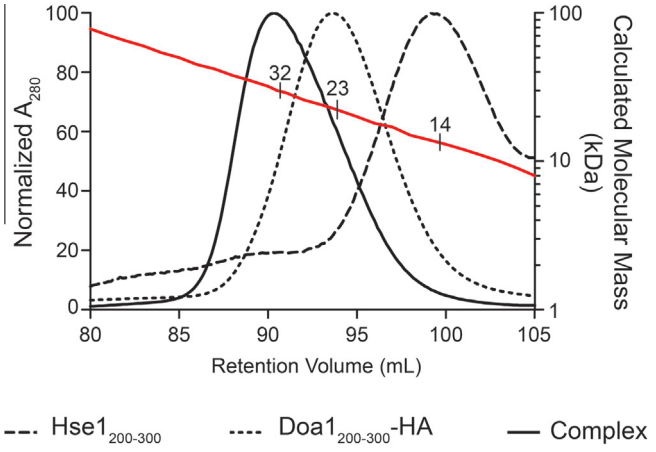

Fig. 2. Size-exclusion chromatograms of Doa1/PFU, Hse1/SH3 and their complex on a Superdex 200 column. Red line indicates a calibration curve for the expected molecular mass of a protein eluted at the corresponding retention volume. Numbers on the red line refer to the calculated molecular masses for Doa1:Hse1 complex, Doa1/PFU and Hse1/SH3, respectively in kDa. (For interpretation of the references to colour in this figure legend, the reader is referred to the web version of this article.)

that Doa1/PFU and Hse1/SH3 interact directly and form a stable complex in solution.

Establishing the direct interaction between Doa1 and Hse1 in solution qualitatively, we further investigated the interaction in a quantitative way. For this purpose, we utilized bio-later interferometry (BLI), an optical technique to assess biomolecular interactions quantitatively [26,27]. His-Doa1$_{296–450}$-HA was immobilized on Ni-NTA sensors and allowed to interact with GST-Hse1$_{200–300}$ at varying concentrations (from 2 to 32 μM) (Fig. 3). We found that GST-Hse1$_{200–300}$ binds to His-Doa1$_{296–450}$-HA with a moderate affinity (K_d) of 5 μM (Table 1). By contrast, GST alone did not bind His-Doa1$_{296–450}$-HA (Fig. S1). Together with the results from size exclusion chromatography and pulldown assay, our data is fully consistent with the previous report [9] and demonstrates that Doa1/PFU interacts directly with Hse1/SH3.

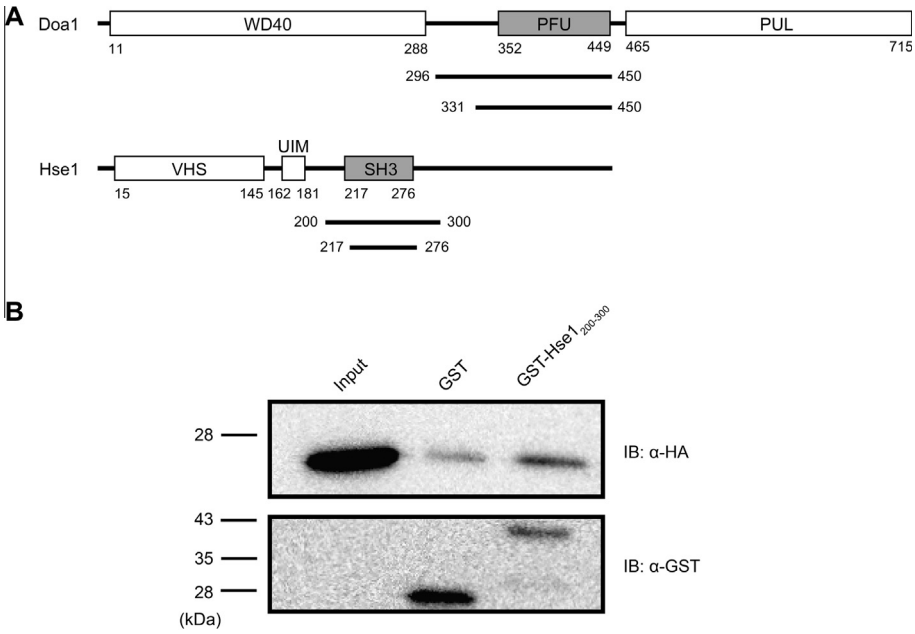

Fig. 1. Direct interaction between Doa1/PFU and Hse1/SH3 *in vitro*. (A) Domain architecture of Doa1 and Hse1. Constructs used for this study are marked by underlines with residue numbers. (B) Pulldown of SH3 domain from Hse1 by GST-PFU domain from Doa1 probed by Western blotting.

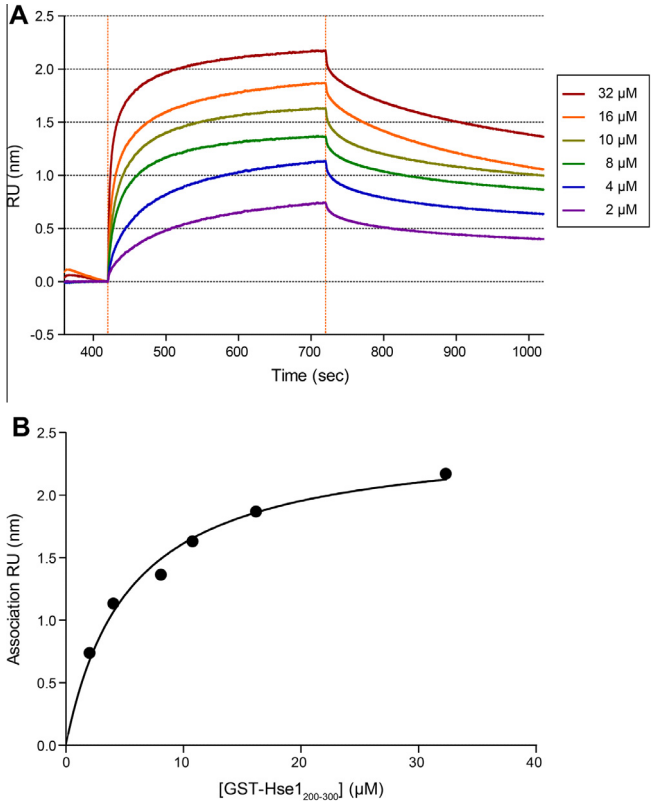

Fig. 3. Quantitative analysis of the direct interaction between Doa1/PFU and Hse1/SH3. (A) BLI sensorgram of association and dissociation between immobilized Doa1/PFU and Hse1/SH3 at various concentrations of Hse1/SH3 from 2 to 32 μM. (B) Steady state analysis of binding was performed using R_{eq} calculated by *BLItz Pro* (ForteBio) with the local fitting option.

Table 1
Dissociation equilibrium constants (K_d) between wild types and mutants of $Doa1_{296–450}$ and $Hse1_{200–300}$.

K_d [a] (μM)	$Doa1_{296–450}$				
	WT	F434A	F434D	N438A	N440A
$Hse1_{200–300}$ WT	5.2 ± 0.97	4.5 ± 1.3	8.5 ± 2.2	n.d.[b]	16 ± 2.6
W254A	n.d.	n.d.	n.d.	n.d.	n.d.

[a] Standard errors of K_d value calculated by *PRISM* (Graphpad Software Inc.).
[b] n.d.: not determined.

To uncover which residues are responsible for the interaction between Doa1/PFU and Hse1/SH3, we attempted to generate a structural model. Previous crystallographic and biochemical studies suggested that the conserved motif F^{434}ILKNTNG^{441} of [9] and the tandem tryptophan residues $W^{254}W^{255}$ of Hse1 are required to interact to each other [9,12]. Using the aforementioned residues as restraints, we modeled a complex between Doa1 and Hse1 with *HADDOCK* [17] (Fig. S2A). Based on the docked model, we hypothesized that F434, N438 and N440 of Doa1 and W254 of Hse1 may be involved in the direct interaction. We then investigated the role of each residue in the interaction by BLI analysis using His-$Doa1_{296–450}$-HA F434A, F434D, N438A and N440A and GST-$Hse1_{200–300}$ W254A. Unexpectedly, we found that N438A of Doa1 and W254A of Hse1 abolished the interaction while F434A and F434D showed no effect on binding (Table 1). Apparently the conserved F434 of Doa1, which was reported to be important in ubiquitin binding via a hydrophobic interaction [5] and predicted to form a putative ubiquitin binding pocket [12], is dispensable in binding Hse1. Based on the results from BLI analysis, we re-generated the docked model for the Doa1/PFU:Hse1/SH3 complex so that N438 and W254 are in direct contact (Fig. S2B). In this re-generated model, Oδ1 in N438 of Doa1 and Nε1 in W254 of Hse1 appear to form a hydrogen bond with the distance of 2.9 Å. Our results suggest that the interaction between Doa1/PFU and Hse1/SH3 is driven mainly by forming a hydrogen bond between N438 of Doa1 and W254 of Hse1.

To obtain structural information of the Doa1/PFU:Hse1/SH3 complex in solution, we determined the solution structure by small-angle X-ray scattering (SAXS). To minimize the potentially negative effects of flexible regions of Doa1 and Hse1 for SAXS analysis, we used truncated constructs, $Doa1_{331–450}$-HA and $Hse1_{217–276}$. The Guininer and pair distance distribution analysis yielded the radius of gyration (R_g) of 26.9 and 28.0 Å, respectively, for the complex (Fig. 4A and Table 2). Maximum diameter of the complex (D_{max}) was estimated to be 90 Å (Fig. 4B). The truncated complex appeared to behave well in solution (Fig. 4C). We then calculated a low-resolution molecular envelope for the Doa1:Hse1 complex and docked the *BUNCH*-derived atomic model of the complex to it (Fig. 4D). Both R_g and D_{max} values from the *BUNCH*-derived model, which are 25 and 91 Å, respectively, are well consistent with those from the Guinier and pair distance distribution analysis. The resulting $Doa1_{331–450}$-HA:$Hse1_{217–276}$ structural model was fitted well ($\chi = 1.60$) to the experimental scattering patterns, evaluated by the *FoXS* webserver [22] (Fig. 4C). Since regions (residues 331–375 and 440–450) are thought to be flexible by a crystallographic study [12] and the *Phyre2* server, we assessed whether the integrity of the complex may be affected by the flexible regions of Doa1 using the conformational dynamics. *EOM* [23,24] suggested four candidate structures for the complex in which the PFU (residues 376–439 of Doa1) and SH3 (residues 217–276 of Hse1) domains remain stable with the flexible region of Doa1 (residues 331–375) being highly dynamic. The *FoXS* webserver implemented with *MES* [25] generated the minimal combination of two models with almost equal population (Fig. 4E). This minimal combination generated by *MES* was fitted well ($\chi = 1.66$) to the experimental scattering profile, also evaluated by the *FoXS* webserver. In this case, both models show R_g values consistent with those determined by SAXS measurements. Taken together, these results demonstrate that Doa1/PFU and Hse1/SH3 can form a stable complex with some alternative conformations in solution.

4. Discussion

The binding affinity of Doa1 with Hse1 is found to be 5 μM by BLI, which is compatible with the interaction of Doa1 with Cdc48 [28], suggesting that the interaction of Doa1 with Hse1 is important in the MVB pathway just as that with Cdc48 in the ERAD pathway. Canonical function of Doa1 in ERAD is mediated by direct interactions with Cdc48 and ubiquitin [5]. Structural and biochemical studies supported the direct interactions between Doa1 and either Cdc48 [28] or ubiquitin [6]. An Armadillo motif in the PUL domain interacts with the C-terminal fragment of Cdc48 with 3.5 μM K_d by ITC [28]. The same Armadillo motif is also involved in the direct interaction between the PUL domain of PLAA, the mammalian ortholog of Doa1, and a peptide derived from the C-terminal region of p97, the mammalian ortholog of Cdc48 with 5 μM K_d by fluorescence polarization [29]. By contrast, the interaction of the PFU domain with ubiquitin is reported to be direct but weak one. For example, the PFU domain of PLAA binds ubiquitin with 1 mM K_d probed by NMR [6]. WD40 domain is also reported to bind to ubiquitin with K_d being 224 μM by NMR [7]. Although binding affinities expressed as K_d values differ from μM to mM range, it is evident that the function of Doa1 in ERAD is exerted by its direct interactions with partner proteins. Our data shows that the involvement of Doa1 in the MVB pathway via Hse1 is

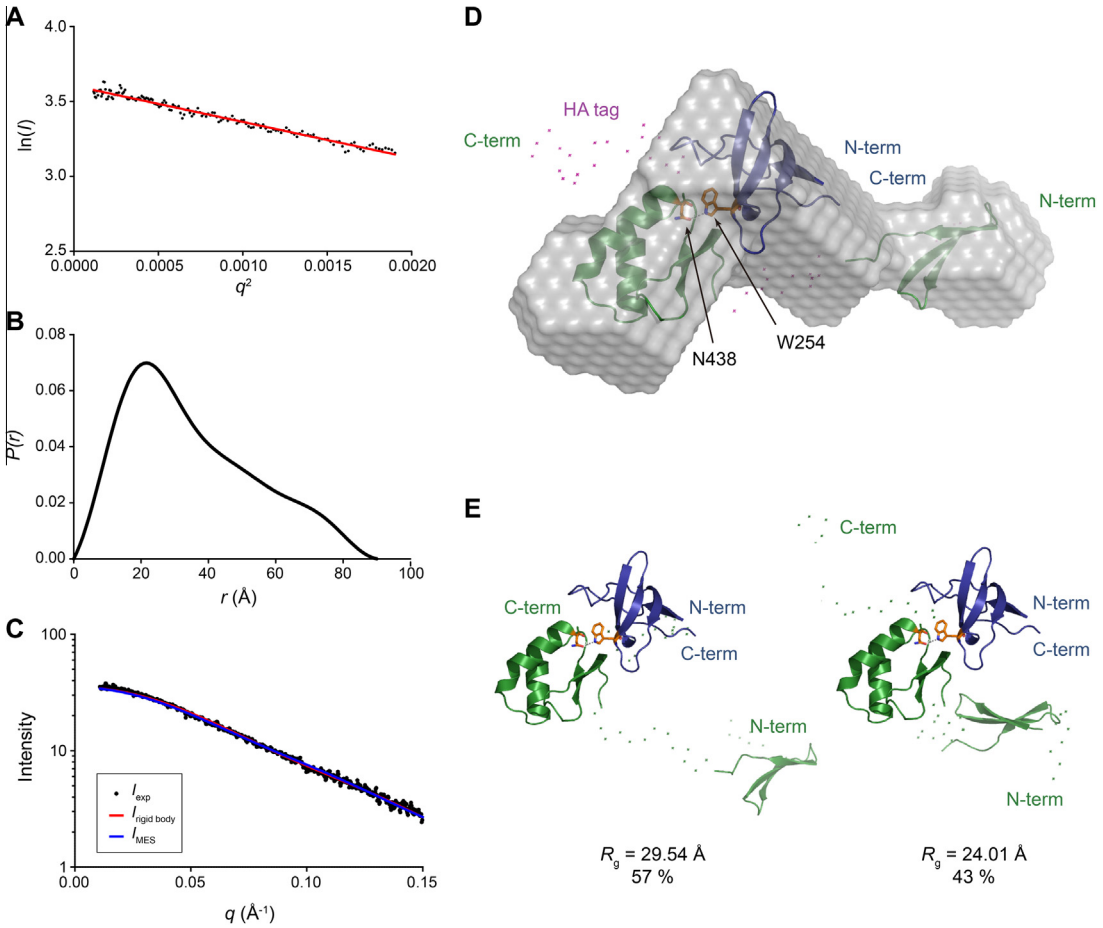

Fig. 4. Solution structure of Doa1/PFU and Hse1/SH3 complex revealed by small-angle X-ray scattering (SAXS). (A) Guinier plot (red) and SAXS data (black) as a function of the magnitude of scattering vectors, $q = (4\pi/\lambda)\sin\theta$, versus the natural logarithm of scattering intensity I, $\ln(I)$. (B) Pair distance distribution function $P(r)$. (C) Rigid body model (red) and conformational dynamic model (blue) are validated against experimental intensities by *FoXS* webserver. (D) *Ab initio* low-resolution envelope with the rigid body model docked. (E) Conformational dynamic models by *EOM* and *FoXS/MES*. Doa1/PFU is colored green, HA-tag of Doa1 magenta, and Hse1/SH3 blue. Key residues involved in the interaction, N438 of Doa1 and W254 of Hse1, are shown as stick models. (For interpretation of the references to colour in this figure legend, the reader is referred to the web version of this article.)

Table 2
SAXS data collection and analysis statistics.

	$Doa1_{331-450}$-HA:$Hse1_{217-276}$
Data-collection parameters	
Synchrotron beamline	PAL-4C
Detector distance (m)	3.0
Wavelength (Å)	1.24
Exposure time (sec)	30
Concentration range (mg/ml)	3.6
Sample parameters	
Polydispersity (%)[a]	13
Structural parameters	
R_g (Å) [from Guinier[b]]	26.9
R_g (Å) [$P(r)$[c]]	28.0
D_{max} (Å)[c]	90.0
Software employed	
Primary data reduction	*An in-house program*
Dara processing	*PRIMUS*
Ab initio analysis	*DAMMIF*
Validation and averaging	*DAMAVER*
Three-dimensional representations	*PyMOL*

[a] Determined by dynamic light scattering.
[b] Experimental curve is trimmed for $qR_g < 1.3$.
[c] Indirect Fourier transform is performed by *GNOM*.

mediated by direct interact between the two proteins, just like the function of Doa1 in the ERAD pathway.

To our surprise, Doa1/PFU interacts with Hse1/SH3 mainly via hydrogen bonding rather than hydrophobic interaction. We found that N438 of Doa1 and W254 of Hse1 are critical residues for the interaction. Interestingly, F434 of Doa1 does not seem to be involved in the interaction with Hse1, contrary to its role in ubiquitin binding [5,12]. An NMR study on the interaction of PFU domain from human homolog of Doa1, PLAA, with ubiquitin showed no significant chemical shift on F450 of PLAA, corresponding to F434 of Doa1 [6]. N454 of PLAA, corresponding to N438 of Doa1, also exhibited little chemical shift upon ubiquitin binding. It appears that key residues of Doa1/PFU in binding ubiquitin and Hse1 are not overlapping, implicating that the small PFU domain may have distinct molecular determinants to specify its binding partners unequivocally using a small number of amino acid side chains.

In this study, we report that Doa1 is involved in endosomal sorting via its direct interaction with Hse1 with a moderate affinity. N438 of Doa1 and W254 of Hse1 are critical in the interaction revealed by quantitative binding analysis, which suggests that the interaction is mediated by hydrogen bonding rather than hydrophobic interactions. We also determined the solution structure of the Doa1/PFU:Hse1/SH3 complex by small-angle X-ray scattering

combined with molecular modeling. Our results identify the chemical nature of the interaction between Doa1/PFU and Hse1/SH3, thereby shedding light on the deeper understanding of the function of Doa1 in the endosomal sorting.

Acknowledgments

We thank the staff at the beamline 4C of Pohang Accelerator Laboratory for technical assistance in collecting SAXS data. This work was supported by Basic Science Research Program (2009-0074586 and 2011-0023402) and the Pioneer Research Center Program (2012-0009597) through the National Research Foundation of Korea (NRF) and the Woo Jang Chun Program (PJ009106) through the Rural Development Agency.

Appendix A. Supplementary data

Supplementary data associated with this article can be found, in the online version, at http://dx.doi.org/10.1016/j.bbrc.2014.02.118.

References

[1] M. Ghislain, R.J. Dohmen, F. Levy, A. Varshavsky, Cdc48p interacts with Ufd3p, a WD repeat protein required for ubiquitin-mediated proteolysis in *Saccharomyces cerevisiae*, EMBO J. 15 (1996) 4884–4899.
[2] E.T. Lis, F.E. Romesberg, Role of Doa1 in the *Saccharomyces cerevisiae* DNA damage response, Mol. Cell. Biol. 26 (2006) 4122–4133.
[3] D. Kunze, D. MacCallum, F.C. Odds, B. Hube, Multiple functions of DOA1 in *Candida albicans*, Microbiology 153 (2007) 1026–1041.
[4] C. Zimmermann, P. Chymkowtich, V. Eldholm, C.D. Putnam, J.M. Lindvall, M. Omerzu, M. Bjoras, R.D. Kolodner, J.M. Enserink, A chemical-genetic screen to unravel the genetic network of *CDC28/CDK1* links ubiquitin and Rad6-Bre1 to cell cycle progression, Proc. Natl. Acad. Sci. USA 108 (2011) 18748–18753.
[5] J.E. Mullally, T. Chernova, K.D. Wilkinson, Doa1 is a Cdc48 adapter that possesses a novel ubiquitin binding domain, Mol. Cell. Biol. 26 (2006) 822–830.
[6] Q.S. Fu, C.J. Zhou, H.C. Gao, Y.J. Jiang, Z.R. Zhou, J. Hong, W.M. Yao, A.X. Song, D.H. Lin, H.Y. Hu, Structural basis for ubiquitin recognition by a novel domain from human phospholipase A2-activating protein, J. Biol. Chem. 284 (2009) 19043–19052.
[7] N. Pashkova, L. Gakhar, S.C. Winistorfer, L. Yu, S. Ramaswamy, R.C. Piper, WD40 repeat propellers define a ubiquitin-binding domain that regulates turnover of F box proteins, Mol. Cell 40 (2010) 433–443.
[8] N.S. Russell, K.D. Wilkinson, Identification of a novel 29-linked polyubiquitin binding protein, Ufd3, using polyubiquitin chain analogues, Biochemistry 43 (2004) 4844–4854.
[9] J. Ren, N. Pashkova, S. Winistorfer, R.C. Piper, DOA1/UFD3 plays a role in sorting ubiquitinated membrane proteins into multivesicular bodies, J. Biol. Chem. 283 (2008) 21599–21611.
[10] J.H. Hurley, ESCRT complexes and the biogenesis of multivesicular bodies, Curr. Opin. Cell Biol. 20 (2008) 4–11.
[11] T. Hou, N. Li, Y. Li, W. Wang, Characterization of domain–peptide interaction interface: prediction of SH3 domain-mediated protein–protein interaction network in yeast by generic structure-based models, J. Proteome Res. 11 (2012) 2982–2995.
[12] R. Nishimasu, H. Komori, Y. Higuchi, H. Nishimasu, H. Hiroaki, Crystal structure of a PFU-PUL domain pair of *Saccharomyces cerevisiae* Doa1/Ufd3, Kobe J. Med. Sci. 56 (2010) E125–E139.
[13] P. Sheffield, S. Garrad, Z. Derewenda, Overcoming expression and purification problems of RhoGDI using a family of "parallel" expression vectors, Protein Expr. Purif. 15 (1999) 34–39.
[14] P. Bradley, K.M. Misura, D. Baker, Toward high-resolution de novo structure prediction for small proteins, Science 309 (2005) 1868–1871.
[15] T.U. Consortium, Activities at the universal protein resource (UniProt), Nucleic Acids Res. 42 (2014) D191–D198.
[16] J. Ko, H. Park, L. Heo, C. Seok, GalaxyWEB server for protein structure prediction and refinement, Nucleic Acids Res. 40 (2012) W294–W297.
[17] S.J.D. Vries, M.V. Dijk, A.M.J.J. Bonvin, The HADDOCK web server for data-driven biomolecular docking, Nat. Protoc. 5 (2010) 883–897.
[18] K. La, S. Mje, Protein structure prediction on the web: a case study using the Phyre server, Nat. Protoc. 4 (2009) 363–371.
[19] D.I. Svergun, Determination of the regularization parameter in indirect-transform methods using perceptual criteria, J. Appl. Crystallogr. 25 (1992) 495–503.
[20] D. Franke, D.I. Svergun, DAMMIF, a program for rapid ab-initio shape determination in small-angle scattering, J. Appl. Cryst. 42 (2009) 342–346.
[21] M.V. Petoukhov, D.I. Svergun, Global rigid body modelling of macromolecular complexes against small-angle scattering data, Biophys. J. 89 (2005) 1237–1250.
[22] D. Schneidman-Duhovny, M. Hammel, A. Sali, FoXS: a web server for rapid computation and fitting of SAXS profiles, Nuclic Acids Res. 38 (Suppl. 2) (2010) W540–W544.
[23] P. Bernado, E. Mylonas, M.V. Petoukhov, M. Blackledge, D.I. Svergun, Structural characterization of flexible proteins using small-angle X-ray scattering, J. Am. Chem. Soc. 129 (2007) 5656–5664.
[24] M.V. Petoukhov, D. Franke, A.V. Shkumatov, G. Tria, A.G. Kikhney, M. Gajda, C. Gorba, H.D.T. Mertens, P.V. Konarev, D.I. Svergun, New developments in the ATSAS program package for small-angle scattering data analysis, J. Appl. Cryst. 45 (2012) 342–350.
[25] M. Pelikan, G.L. Hura, M. Hammel, Structure and flexibility within proteins as identified through small angle X-ray scattering, Gen. Physiol. Biophys. 28 (2009) 174–189.
[26] J. Concepcion, K. Witte, C. Wartchow, S. Choo, D. Yao, H. Persson, J. Wei, P. Li, B. Heidecker, W. Ma, R. Varma, L.S. Zhao, D. Perillat, G. Carricato, M. Recknor, K. Du, H. Ho, T. Ellis, J. Gamez, M. Howes, J. Phi-Wilson, S. Lockhard, R. Zuk, H. Tan, Label-free detection of biomolecular interactions using biolayer interferometry for kinetic characterization, Comb. Chem. High Throughput Screen 12 (2009) 791–800.
[27] M. Citartan, S.C. Gopinath, J. Tominaga, T.H. Tang, Label-free methods of reporting biomolecular interactions by optical sensors, Analyst 138 (2013) 3576–3592.
[28] G. Zhao, G. Li, H. Schindelin, W.J. Lennarz, An Armadillo motif in Ufd3 interacts with Cdc48 and is involved in ubiquitin homeostasis and protein degradation, Proc. Natl. Acad. Sci. USA 106 (2009) 16197–16202.
[29] L. Qiu, N. Pashkova, J.R. Walker, S. Winistorfer, A. Allali-Hassani, M. Akutsu, R. Piper, S. Dhe-Paganon, Structure and function of the PLAA/Ufd3-p97/Cdc48 complex, J. Biol. Chem. 285 (2010) 365–372.